CITATION

DOI

COPYRIGHT

USAGE

A Possible Submarine Landslide and Associated Tsunami at the Northwest Nile Delta, Mediterranean Sea

BY AHMET C. YALCINER, ANDREY ZAYTSEV,
BETUL AYTORE, ISIL INSEL, MOHAMMAD HEIDARZADEH,
ROZITA KIAN, AND FUMIHIKO IMAMURA
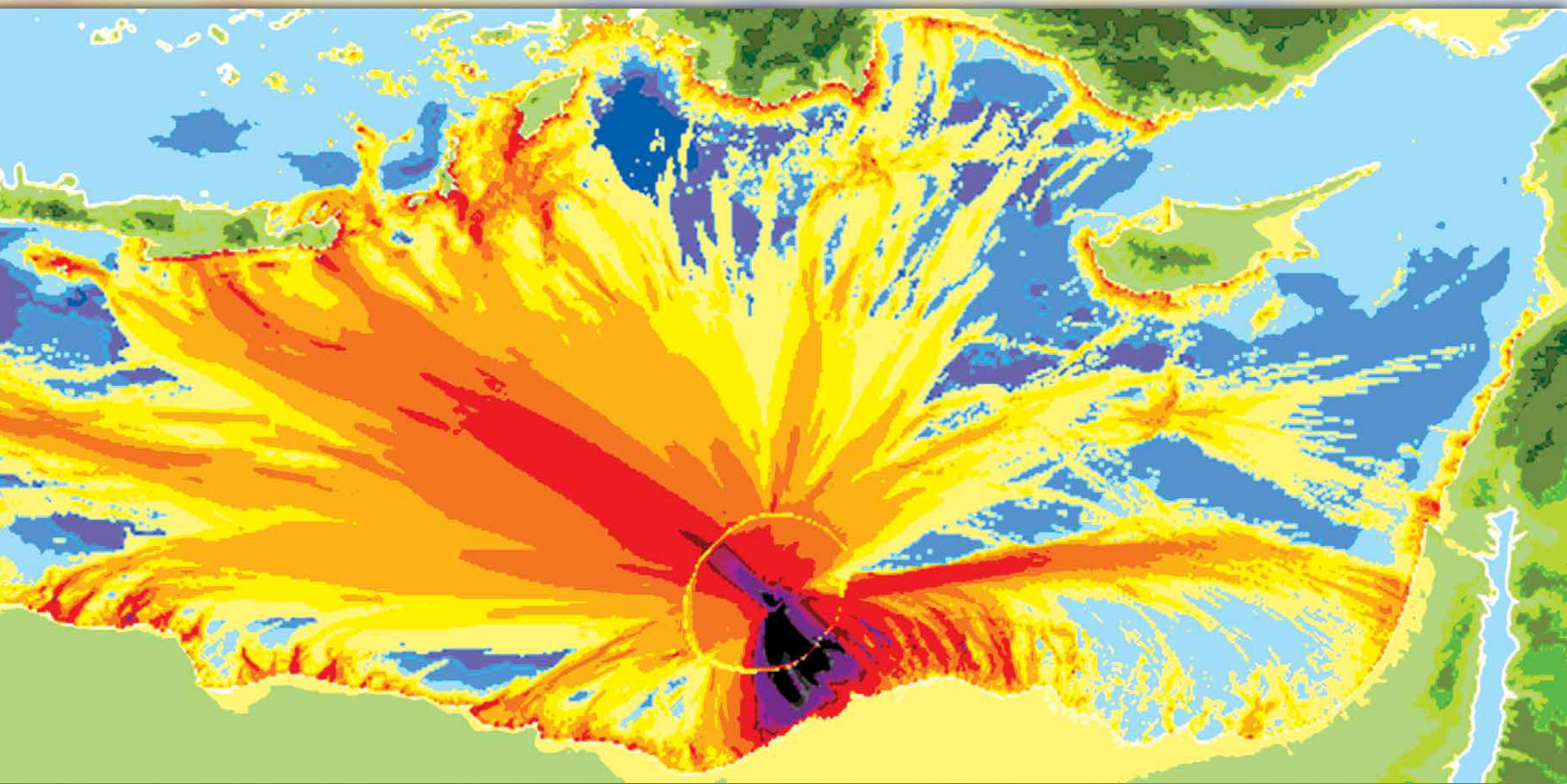
ABSTRACT. A hypothetical landslide tsunami at the Nile Delta in the Eastern Mediterranean Sea is modeled in order to study hazards it would pose to the region. The methodology used is based on numerical simulation of the generation and propagation of a realistic landslide scenario. The volume of the landslide source is 41 km^3, located offshore northern Egypt. The maximum simulated wave heights along the northern, southern, and eastern coasts in the region are in the range of 1–12, 1–6.5, and 0.5–3 m, respectively. The maximum tsunami current velocity along the coasts reaches ~ 2–5 m s^{-1}. Simulations show that bathymetric features in the region and the coastal morphology focus the maximum tsunami waves into some specific paths along which the largest tsunami runup heights occur. The semi-enclosed nature of the eastern Mediterranean causes wave reflections, which result in several wave trains arriving at every coastal site. In some coastal sites, the largest simulated wave belongs to the second wave train, indicating that wave reflection is responsible for this delayed large wave. Based on the results, deployment of a network of deepwater pressure gauges may help in detection and early warning of possible landslide-generated tsunamis in the Eastern Mediterranean.

INTRODUCTION

Large hazards posed by landslide-generated waves have attracted the attention of the scientific community in recent years (e.g., Synolakis et al., 2002, Yalciner et al., 2003; Bardet et al., 2003). Unlike tectonic tsunamis, which often follow noticeable shaking caused by moderate/large earthquakes, landslide-generated waves may occur without any advance alarm, making them a major hazard to coastal communities (Heidarzadeh et al., 2014). Thus, it is important to identify coastal communities that may be affected by submarine landslides and study the associated risks.

Here, we investigate the hazards from submarine landslide-generated tsunamis offshore of the Nile River delta (Figure 1) through numerical modeling of a possible landslide source. As the world's longest river, the Nile carries a large sediment load, and the area offshore the Nile Delta in the Eastern Mediterranean Sea where these sediments are deposited is known as the Nile deep-sea turbidite system (NDSTS; Heidarzadeh et al., 2014). The dimensions of the sedimented area is estimated to be 600 km × 300 km (Ducassou et al., 2009), indicating its potential as a source of large-scale submarine mass failure. In addition, the Eastern Mediterranean Sea is a complex tectonic zone that includes the edges of three plates, the African, the Arabian, and the Anatolian (Figure 1). Hence, the region is subject to many earthquakes (El-Sayed et al., 2004). The combination of high sedimentation rates and high seismicity makes the area susceptible to underwater landslides that could potentially generate tsunamis. By simulating realistic landslide volumes as possible tsunami sources, we produce tsunami runup heights along the region's coast.

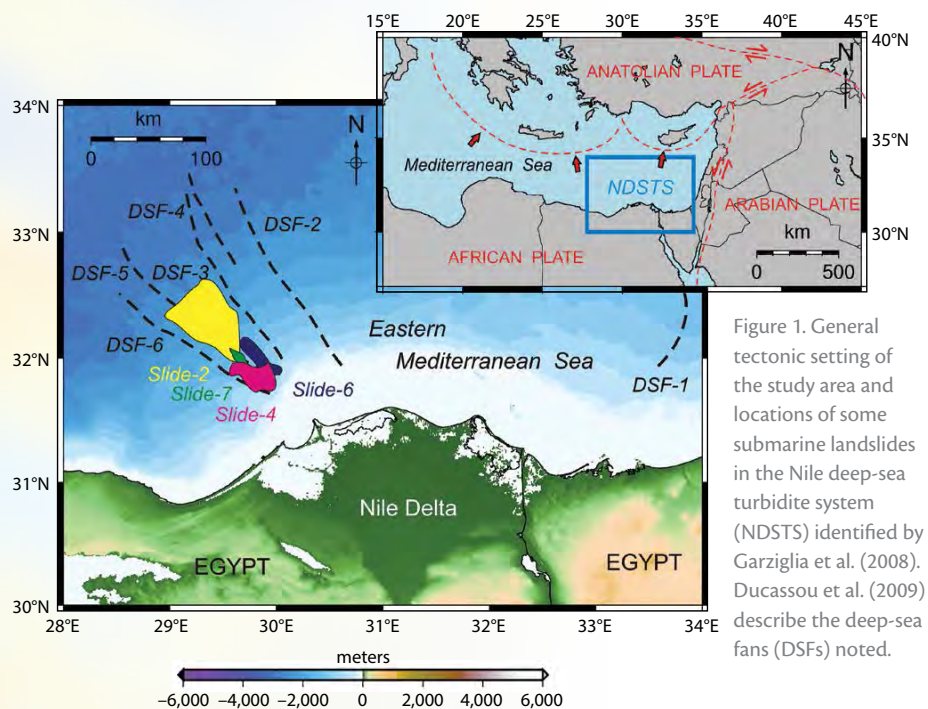## POTENTIAL FOR SUBMARINE LANDSLIDES OFFSHORE THE NILE DELTA

Several researchers have studied submarine mass transports and slope failures on the Nile River delta. Using an extensive bathymetric survey and seismic profiling, Loncke et al. (2002) showed that the NDSTS is extremely vulnerable to mass-wasting events and has had several slope failures in the past; the failures were possibly triggered by seismic activity, gas seep instabilities, mud volcanoes, and salt-related faults. Ducassou et al. (2009) identified six deep-sea fans (DSF) offshore the Nile Delta (Figure 1), each of which includes a large canyon with walls that are susceptible to failure, and they reported several large-scale submarine slope failures over the last 200,000 years.

Garziglia et al. (2008) identified seven mass-transport deposits in the western part of the NDSTS with thicknesses ranging from 10 m to 70 m and volumes between 3 km³ and 500 km³ (Figure 1).

The volumes of slides labeled 2, 4, 6, and 7 in Figure 1 were 500 km³, 63 km³, 14 km³, and 2.5 km³, respectively. Garziglia et al. (2008) speculated that the main trigger for these mass failures might have been large remote or even moderate local earthquakes. Loncke et al. (2009) showed that the NDSTS is the locus of many submarine failures and identified three classifications for the possible slope failures there: (1) numerous localized slides generated by gravity spreading, (2) giant mass movements triggered by earthquakes or fluid/climate/eustatic oscillations, and (3) thin-skinned slides on steep slopes and localized levee liquefactions triggered by earthquake shaking.

METHODOLOGY AND DATA

We numerically model tsunami waves by assuming realistic landslide scenarios. We use two different models to simulate tsunami generation, propagation, and runup: TWO LAYER (Imamura and Imteaz, 1995; Yalciner et al., 2002) for

Figure 1. General tectonic setting of the study area and locations of some submarine landslides in the Nile deep-sea turbidite system (NDSTS) identified by Garziglia et al. (2008). Ducassou et al. (2009) describe the deep-sea fans (DSFs) noted.
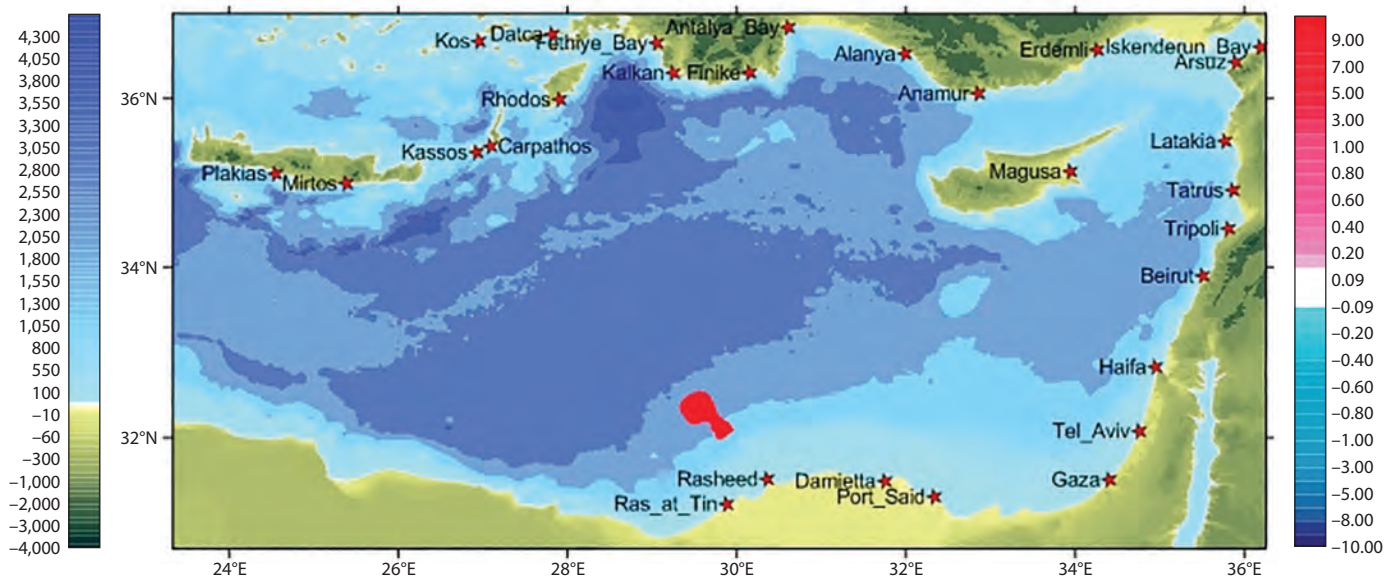
Figure 2. The study domain and locations of selected numerical gauge points as well as the landslide area (red polygon).

modeling landslide generation and NAMI DANCE for modeling tsunami propagation and runup. Until recently, it was common to apply a static dipole wave as the initial condition for tsunami simulations (not only for the slide-generated waves but also for solid block models; Harbitz, 1992; Bondevik et al., 2005a,b). This kind of approximation is acceptable for tectonic tsunamis with a high source speed (Heidarzadeh et al., 2014). However, the kinematic characteristics of mass flows on the seafloor due to landslides or slumps necessitate use of different types of initial wave profiles that take into account the slow

generation velocity of seafloor landslides. Therefore, it is important to incorporate the slow movement at the ocean floor into the mathematical modeling.

TWO LAYER (Imamura and Imteaz, 1995) solves nonlinear long-wave equations using the finite difference technique and following the leap-frog solution procedure within two interfacing layers with appropriate kinematic and dynamic boundary conditions at the seabed, interface, and water surface. The two interfacing layers are the water body and the mass moving at the bottom. When TWO LAYER tests the volume/size of the slide mass and the bottom slope in a

regular-shaped basin, it is observed that after a certain time period, the landslide movement becomes very slow and then stops. Water surface elevation and discharge fluxes are stored in files generated by TWO LAYER when the landslide stops (approximately five to six minutes after its start). These files are then used as initial conditions in simulations that compute wave propagation and coastal amplification. NAMI DANCE is used in the simulations. NAMI DANCE is a numerical tool that solves the nonlinear form of shallow-water equations using the necessary initial conditions: water elevations and discharge fluxes computed by the TWO LAYER model (Insel, 2009). NAMI DANCE was developed specifically for tsunami modeling (Yalciner et al., 2006), and it has been tested and validated for research and operational purposes (Zahibo et al., 2003; Ozer and Yalciner, 2011; Yalciner et al., 2006, 2007, 2010, in press; Onat and Yalciner, 2013). The model simulates tsunami wave propagation by using a finite difference leap-frog scheme for basins of irregular shape and bathymetry in nested domains, and computes water elevations, runup,

Ahmet C. Yalciner *is Professor, Ocean Engineering Research Center, Department of Civil Engineering, Middle East Technical University (METU), Ankara, Turkey.* **Andrey Zaytsev** *is Head, Laboratory of Special Research Bureau for Automation of Marine Research, Far Eastern Branch of Russian Academy of Sciences, Uzhno-Sakhalinsk, Russia, and Associate Professor, Nizhniy Novgorod State Technical University, Nizhny Novgorod, Russia.* **Betul Aytore** *is Research/Project Assistant, Ocean Engineering Research Center, Department of Civil Engineering, METU, Ankara, Turkey.* **Isil Insel** *is Research/Project Assistant, Ocean Engineering Research Center, Department of Civil Engineering, METU, Ankara, Turkey.* **Mohammad Heidarzadeh** *is Research Associate, Earthquake Research Institute, University of Tokyo, Tokyo, Japan.* **Rozita Kian** *is Research/Project Assistant, Ocean Engineering Research Center, Department of Civil Engineering, METU, Ankara, Turkey.* **Fumihiko Imamura** *is Professor of Tsunami Engineering, International Research Institute of Disaster Science, Tohoku University, Sendai, Japan.*

flow depths, and depth-averaged current velocities in the simulation domain.

Simulations were performed covering a period of 240 minutes. The time steps for modeling of generation (by TWO LAYER) and propagation (by NAMI DANCE) phases were 0.005 s and 3 s, respectively. The computational domain for our simulations is 23.338°E–36.255°E and 30.689°N–37.003°N with a grid spacing of 200 m (Figure 2). Among the landslides identified by Garziglia et al. (2008) in Figure 1, slide 2 is the largest and potentially the most hazardous in the region. Therefore, it was chosen as the initial source for our modeling. However, we applied a moderate slide volume compared to that of the real slide 2 volume of 500 km^3 because such a large slide is an extreme and rare event. Our study was aimed at modeling a landslide with moderate volumes in the region. The surface area of the selected landslide scenario is ~ 1,575 km^2 and the volume is ~ 41 km^3. The density of slide material is assumed as 1,800 km m^{-3}. The average thickness is 60 m and the runout distance is 77 km in a southeast to northwest direction (Figure 2). To compare this slide with other actual catastrophic landslide tsunamis in the world, we note that the volume of the 1998 Papua New Guinea landslide tsunami was ~ 4–7 km^3, resulting in a death toll of 2,200 in the nearest coastal village (Watts et al., 1999; Tappin et al., 2001; Okal et al., 2001, 2002; Borrero et al., 2002, 2003; Synolakis et al., 2002; Lynett et al., 2003).

SIMULATION RESULTS

Figures 3–6 and Table 1 show the results of the tsunami simulations. Snapshots of tsunami propagation show that the tsunami waves reach Eastern Mediterranean coasts about one hour after the landslide (Figure 3). They demonstrate that
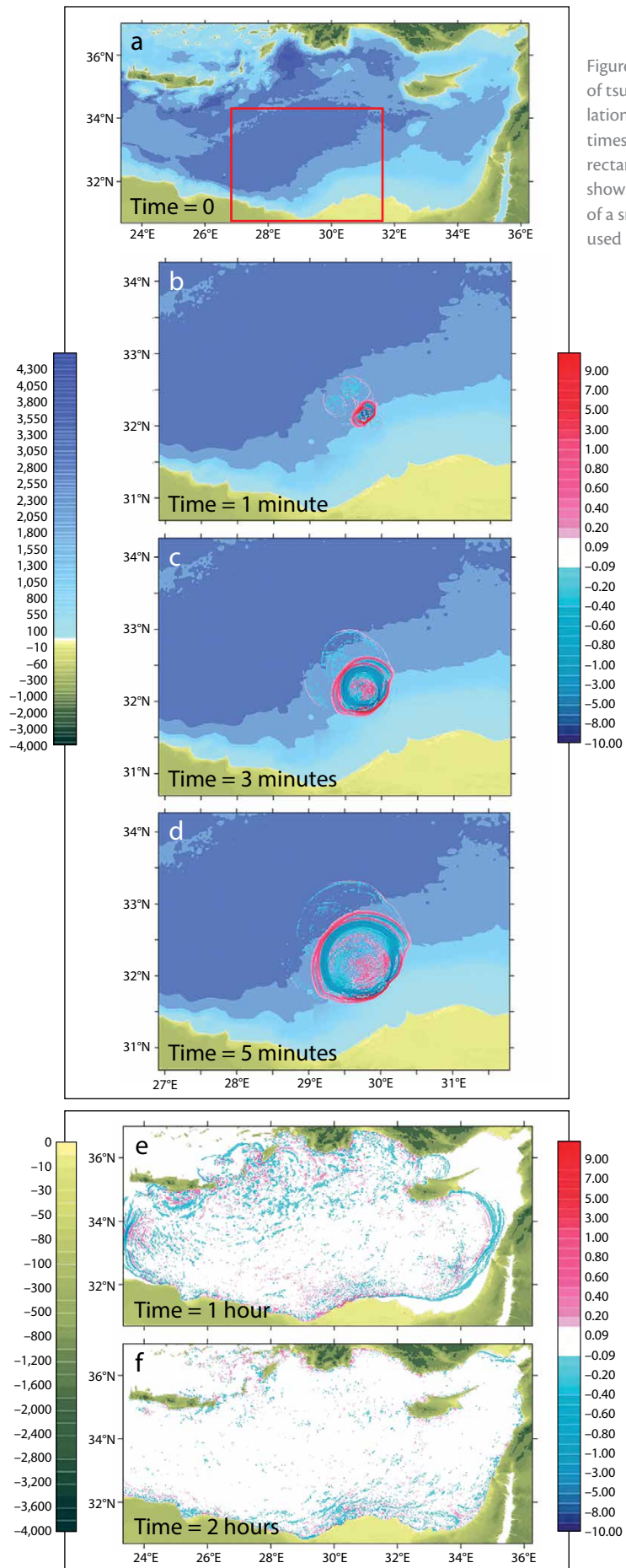

Figure 3. Snapshots of tsunami simulations at different times. The red rectangle in panel a shows the borders of a smaller domain used in panels b–d.

Cyprus acts as a shield protecting the Syrian and southern Turkish coasts, which receive relatively smaller tsunami waves compared to Cyprus (Figure 4).

Figure 4 also shows the distribution of maximum wave heights along different coastlines in the region (bar plots) as well as maximum tsunami wave amplitudes in each computational grid point over the entire tsunami simulation time (color map). In fact, it presents a deterministic tsunami hazard assessment for the region based on the landslide scenario we used. The color map in Figure 4 clearly indicates that the largest tsunami waves are funneled along specific paths in the region. These paths are usually forced by two factors: (1) the orientation of the landslide, and (2) morphological features in the region (e.g., Satake 1988). According to the results displayed in Figure 4, maximum tsunami waves are directed along about eight preferential paths that result in

Table 1. Maximum positive and negative wave amplitudes and arrival times of initial and maximum waves at selected numerical gauge points along with their water depths and coordinates.

City	Water depth (m)	Long. (°N)	Lat. (°W)	Arrival time of initial wave (min)	Arrival time of max. wave (min)	Max. (+) wave amplitude (m)	Max. (−) wave amplitude (m)
Ras at Tin	4.0	29.882	31.215	21	22	4.0	−2.0
Rasheed	2.8	30.360	31.510	36	37	2.3	−1.4
Damietta	3.3	31.750	31.485	88	98	0.6	−0.5
Port Said	4.0	32.338	31.302	83	221	0.4	−0.4
Gaza	3.0	34.403	31.504	81	186	0.6	−0.7
Tel Aviv	2.0	34.759	32.075	75	88	1.0	−1.1
Haifa	6.0	34.949	32.835	62	74	0.6	−0.9
Beirut	−1.0	35.509	33.903	70	70	1.0	0.0
Tripoli	2.0	35.812	34.459	74	83	0.6	−0.7
Tatrus	3.0	35.864	34.913	74	106	0.4	−0.6
Latakia	10.0	35.772	35.493	78	87	0.5	−0.4
Gazimagusa	10.0	33.946	35.136	28	167	0.4	−0.4
Arsuz	3.0	35.896	36.427	88	216	0.3	−0.2
Iskenderun Bay	8.0	36.189	36.604	47	220	0.2	−0.2
Erdemli	3.0	34.262	36.569	48	130	0.3	−0.3
Anamur	6.0	32.858	36.056	53	71	0.8	−0.7
Alanya	20.0	31.991	36.524	46	70	0.8	−1.1
Antalya Bay	7.0	30.612	36.836	33	84	0.9	−0.8
Finike	6.0	30.155	36.300	42	62	1.1	−2.1
Kalkan	9.0	29.252	36.297	37	49	1.4	−2.8
Fethiye Bay	9.0	29.054	36.653	42	84	1.0	−0.8
Datca	20.0	27.821	36.756	62	201	0.5	−0.6
Rhodos	−0.5	27.910	35.983	40	67	2.0	0.0
Kos	5.0	26.955	36.672	61	112	0.7	−0.6
Carpathos	10.0	27.092	35.432	38	55	1.8	−1.9
Kassos	20.0	26.928	35.360	35	48	1.2	−1.9
Mirtos	10.0	25.388	34.993	46	65	2.7	−2.9
Plakias	10.0	24.553	35.107	53	81	1.0	−0.8

maximum coastal runup heights. For example, the maximum calculated runup height is ~ 12 m, which is generated by the strongest tsunami energy path. The runup heights along northern, southern, and eastern coasts are in the range of 1–12 m, 1–6.5 m, and 0.5–3 m, respectively. In the simulation, computed maximum current velocities reached 2–5 m s^{-1} along the coast. As the region's coastal areas are heavily populated, such large runup heights along with high current velocities of ~ 5 m s^{-1} can be catastrophic.

Figure 5 plots the oscillations of tsunami waves at selected coastal sites in the region. This figure shows that tsunami waves are composed of several wave trains that result from multiple wave reflections because the Mediterranean is a semi-enclosed basin. Some of these late wave trains contain high energy and can be hazardous. For example, at two stations, Anamur and Antalya Bay, Figure 5 shows that the largest wave occurs in the second wave train. Table 1 demonstrates that, at Datca, the first tsunami waves arrive 62 minutes after slope failure, and the largest waves arrive at this station after 201 minutes. This behavior can be observed at some other stations, such as Port Said and Arsuz. Table 1 indicates that the travel times of possible tsunamis to Turkish and Greek coasts are around one hour.

DISCUSSION

Although submarine landslides with volumes of up to 500 km^3 are identified in the Nile Delta (Garziglia et al., 2008), we modeled tsunami generation by using a reasonable but significant size landslide with a volume of 41 km^3. The simulated runup heights were up to ~ 12 m along the nearest coastal areas. Such large runup heights have the potential

to produce significant damage and yield high death tolls; hence, tsunami mitigation measures are necessary. However, options for landslide tsunami countermeasures are limited in comparison to tectonic (earthquake-generated) tsunamis for several reasons. First, usually there are no precursors (e.g., an earthquake) warning of the possible arrival of landslide tsunamis unless they are caused by instabilities resulting from earthquake shaking. Second, landslide tsunamis usually produce larger wave heights on adjacent coastlines than tectonic tsunamis, which generate smaller events locally. Third, tectonic tsunamis usually occur along subduction zones

whereas landslide tsunamis can occur in other specific circumstances such as high sedimentation rates. Therefore, construction of coastal protection structures intended to mitigate the effects of tectonic tsunamis may not provide effective protection against landslide tsunamis that have greater wave amplitudes.

Because our knowledge of landslide tsunamis is not as great as for tectonic events, it is not certain when and where landslide tsunamis are going to occur. Accordingly, countermeasures for landslide tsunamis are not as well developed as for tectonic events. In the case of the Eastern Mediterranean, our simulations show that, if the Nile Delta
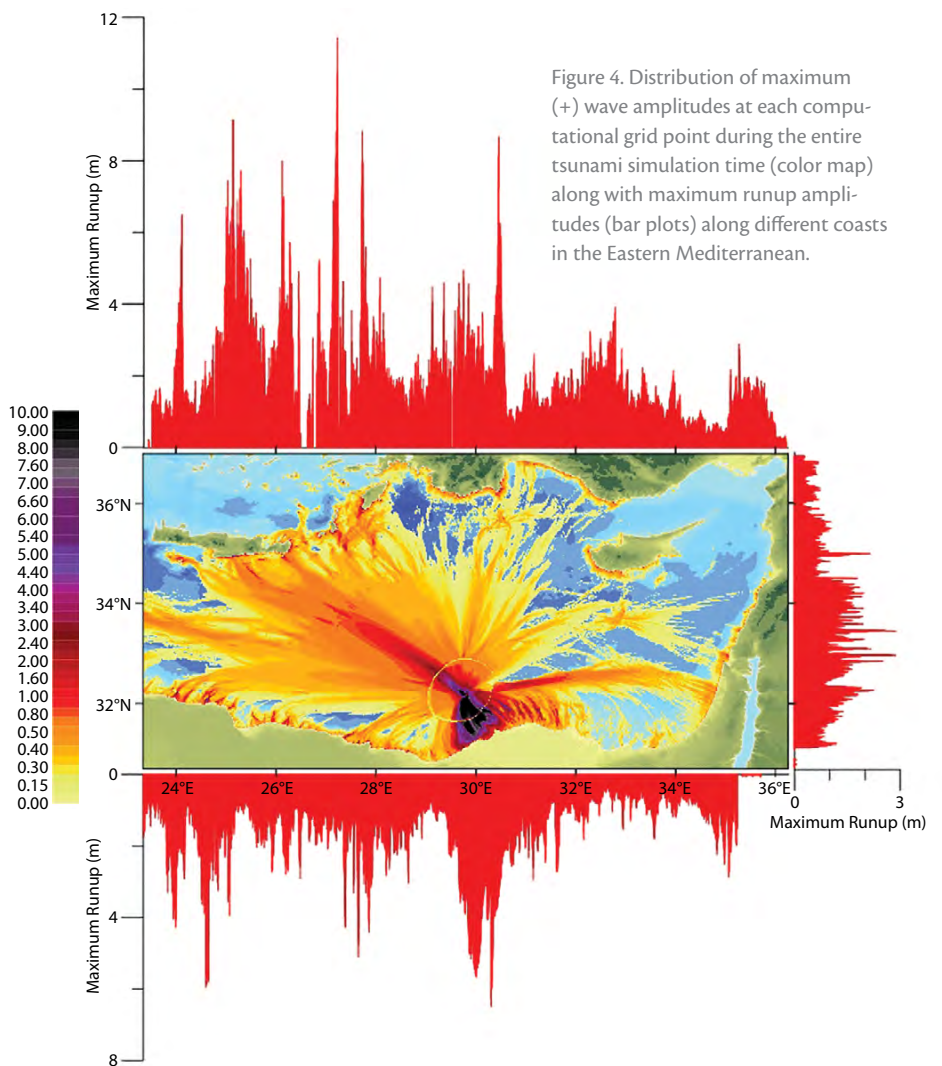

Figure 4. Distribution of maximum (+) wave amplitudes at each computational grid point during the entire tsunami simulation time (color map) along with maximum runup amplitudes (bar plots) along different coasts in the Eastern Mediterranean.
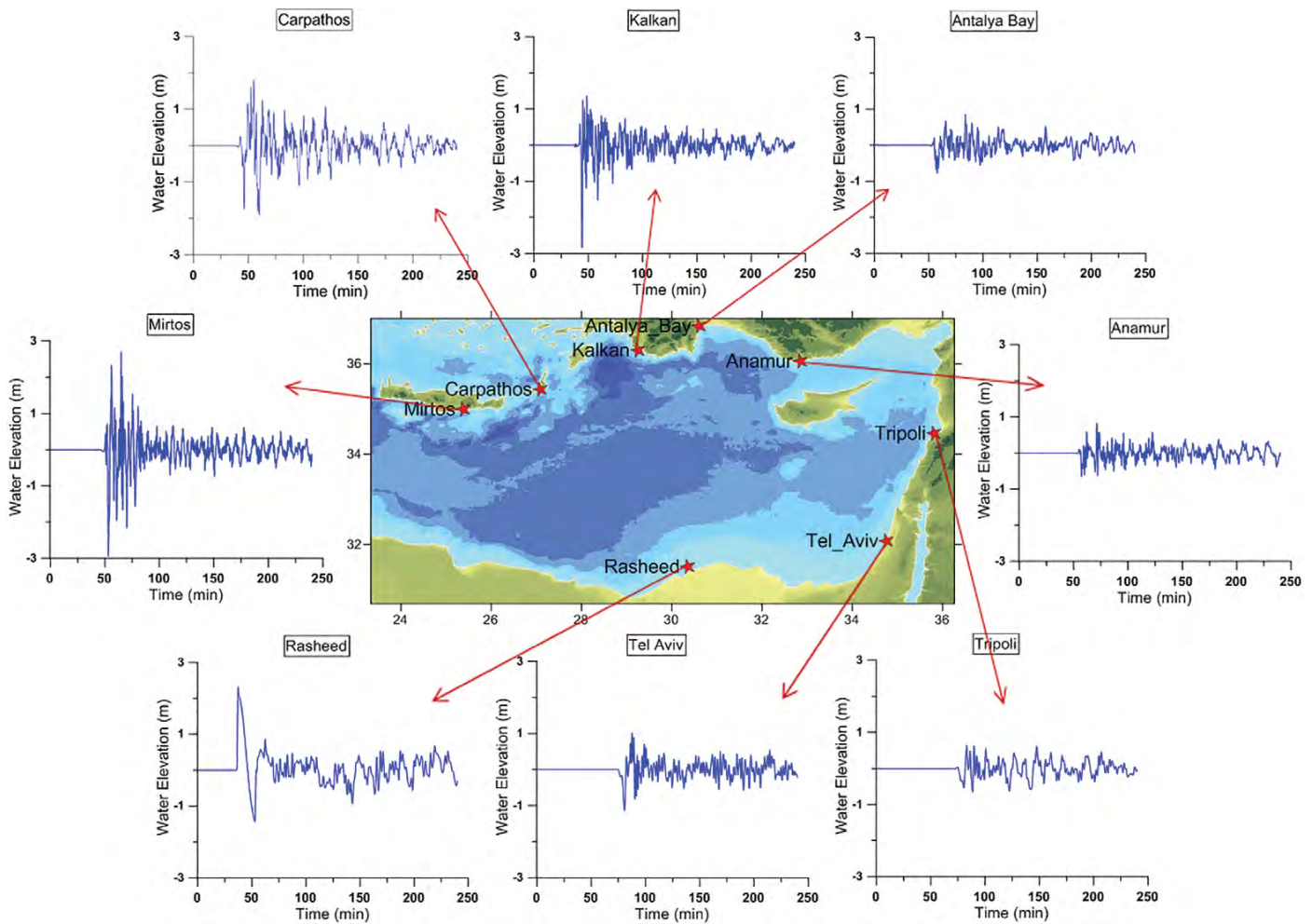
Figure 5. Time histories of water surface fluctuations at different numerical gauge points.

is the landslide source, it may take only about an hour for the resulting tsunami waves to reach the northern coasts of the Eastern Mediterranean. A network of deepwater pressure gauges offshore of these areas may help detect the tsunamis early enough to give timely warnings to threatened coastal communities in the Eastern Mediterranean.

CONCLUSIONS

Our scenario-based landslide tsunami hazard assessment reveals several aspects of tsunami hazards posed by possible submarine landslides in the region:

For a landslide volume of 41 km³, maximum wave heights along the

northern, southern, and eastern coasts are in the range 1–12 m, 1–6.5 m, and 0.5–3 m, respectively. Maximum tsunami current velocity along coastal areas may reach as high as 2–5 m s⁻¹.

Bathymetric features in the region help to focus tsunami energy into specific paths. Therefore, the largest tsunami runup heights occur along the coastlines that intersect these paths.

The semi-enclosed nature of the Eastern Mediterranean causes several wave reflections, which result in multiple wave trains reaching every coastal site. In some coastal sites, the largest waves occur in the second wave train, indicating that wave reflection is responsible.

A network of deepwater pressure gauges may be useful for detection and early warning of possible landslide tsunamis for the Turkish and Greek coasts.

REFERENCES

Bardet, J.-P., C.E. Synolakis, H.L. Davies, F. Imamura, and E.A. Okal. 2003. Landslide tsunamis: Recent findings and research directions. *Pure and Applied Geophysics* 160:1,793–1,809, http://dx.doi.org/10.1007/s00024-003-2406-0.

Bondevik, S., F. Lovholt, C. Harbitz, J. Mangerud, D. Alastair, and J.I. Svendsen. 2005a. The Storegga Slide tsunami: Comparing field observations with numerical simulations. *Marine and Petroleum Geology* 22:195–208, http://dx.doi.org/10.1016/j.marpetgeo.2004.10.003.

Bondevik, S., J. Mangerud, S. Dawson, D. Alastair, and O. Lohne. 2005b. Evidence for three North Sea tsunamis at the Shetland Islands between 8000 and 1500 years ago. *Quaternary Science Reviews* 24:1,757–1,775, http://dx.doi.org/10.1016/j.quascirev.2004.10.018.

Borrero, J.C., J. Bu, C. Saiang, B. Uslu, J. Freckman, B. Gomer, E.A. Okal, and C.E. Synolakis. 2003. Field survey and preliminary modeling of the Wewak, Papua New Guinea earthquake and tsunami of 9 September 2002. *Seismological Research Letters* 74:393–405, http://dx.doi.org/10.1785/gssrl.74.4.393.

Borrero, J.C., H. Davies, B. Uslu, E. Okal, and C. Synolakis. 2002. Preliminary modeling of tsunami waves generated by the earthquake of 9 September 2002 offshore of northern Papua New Guinea. Paper presented at the 2002 fall meeting of the American Geophysical Union, Abstract #S62C-1213 available at http://adsabs.harvard.edu/abs/2002AGUFM.S62C1213B.

Ducassou, E., S. Migeon, T. Mulder, A. Murat, L. Capotondi, S.M. Bernasconi, and J. Mascle. 2009. Evolution of the Nile deep-sea turbidite system during the Late Quaternary: Influence of climate change on fan sedimentation. *Sedimentology* 56:2,061–2,090, http://dx.doi.org/10.1111/j.1365-3091.2009.01070.x.

El-Sayed, A., I. Korrat, and H.M. Hussein. 2004. Seismicity and seismic hazard in Alexandria (Egypt) and its surroundings. *Pure and Applied Geophysics* 161:1,003–1,019, http://dx.doi.org/10.1007/s00024-003-2488-8.

Garziglia, S., S. Migeon, E. Ducassou, L. Loncke, and J. Mascle. 2008. Mass-transport deposits on the Rosetta province (NW Nile deep-sea turbidite system, Egyptian margin): Characteristics, distribution, and potential causal processes. *Marine Geology* 250:180–198, http://dx.doi.org/10.1016/j.margeo.2008.01.016.

Harbitz, C.B. 1992. Model simulations of tsunamis generated by the Storegga Slides. *Marine Geology* 105:1–21, http://dx.doi.org/10.1016/0025-3227(92)90178-K.

Heidarzadeh, M., S. Krastel, and A.C. Yalciner. 2014. The state-of-the-art numerical tools for modeling landslide tsunamis: A short review. Pp. 483–495 in *Submarine Mass Movements and Their Consequences*. Advances in Natural and Technological Hazards Research, vol. 37, http://dx.doi.org/10.1007/978-3-319-00972-8_43.

Imamura, F., and M.M.A. Imteaz. 1995. Long waves in two-layers: Governing equations and numerical model. *Science of Tsunami Hazards* 13:3–24.

Insel, I. 2009. The effects of the material density and dimensions of the landslide on the generated tsunamis. M.Sc. Thesis, Middle East Technical University, Department of Civil Engineering, Coastal and Ocean Engineering Division.

Loncke, L., V. Gaullier, G. Bellaiche, and J. Mascle. 2002. Recent depositional patterns of the Nile deep-sea fan from echo-character mapping. *AAPG Bulletin* 86:1,165–1,186, http://dx.doi.org/10.1306/61EEDC42-173E-11D7-8645000102C1865D.

Loncke, L., V. Gaullier, L. Droz, E. Ducassou, S. Migeon, and J. Mascle. 2009. Multi-scale slope instabilities along the Nile deep-sea fan, Egyptian margin: A general overview. *Marine and Petroleum Geology* 26:633–646, http://dx.doi.org/10.1016/j.marpetgeo.2008.03.010.

Lynett, P.J., J.C. Borrero, P.L.-F. Liu, and C.E. Synolakis. 2003. Field survey and numerical simulations: A Review of the 1998 Papua New Guinea tsunami. *Pure and Applied Geophysics* 160:2,119–2,146, http://dx.doi.org/10.1007/s00024-003-2422-0.

Okal, E., J. Borrero, and C. Synolakis. 2002. Solving the puzzle of the 1998 Papua New Guinea tsunami: The case for a slump. Pp. 863–877 in *Proceedings of the Solutions to Coastal Disasters '02*, http://dx.doi.org/10.1061/40605(258)74.

Okal, E., and C. Synolakis. 2001. Comment on "Origin of the 17 July 1998 Papua New Guinea Tsunami: Earthquake or Landslide?" by E.L. Geist. *Seismological Research Letters* 72:362–366.

Onat, Y., and A.C. Yalciner. 2013. Initial stage of database development for tsunami warning system along Turkish coasts. *Ocean Engineering* 74:141–154, http://dx.doi.org/10.1016/j.oceaneng.2013.09.008.

Ozer, C., and A.C. Yalciner. 2011. Sensitivity study of hydrodynamic parameters during numerical simulations of tsunami inundation. *Pure and Applied Geophysics* 168:2,083–2,095, http://dx.doi.org/10.1007/s00024-011-0290-6.

Satake, K. 1988. Effects of bathymetry on tsunami propagation: Application of ray tracing to tsunamis. *Pure and Applied Geophysics* 126:27–36, http://dx.doi.org/10.1007/BF00876912.

Synolakis, C.E., J.-P. Bardet, J.C. Borrero, H.L. Davies, E.A. Okal, E.A. Silver, S. Sweet, and D.R. Tappin. 2002. The slump origin of the 1998 Papua New Guinea tsunami. *Proceedings of the Royal Society of London Series A* 458:763–789, http://dx.doi.org/10.1098/rspa.2001.0915.

Tappin, D.R., P. Watts, G.M. McMurtry, Y. Lafoy, and T. Matsumoto. 2001. The Sissano Papua New Guinea tsunami of July 1998: Offshore evidence on the source mechanism. *Marine Geology* 175:1–23, http://dx.doi.org/10.1016/S0025-3227(01)00131-1.

Watts, P., C.C. Borrero, D.R. Tappin, J.-P. Bardet, S.T. Grilli, and C.E. Synolakis. 1999. Novel simulation technique employed on the 1998 Papua New Guinea Tsunami. Paper presented at the 1999 IUGG General Assembly, Birmingham, UK. http://appliedfluids.com/IUGG.pdf.

Yalciner, A.C., B. Alpar, Y. Altınok, İ. Özbay, and F. Imamura. 2002. Tsunamis in the Sea of Marmara: Historical documents for the past, models for the future. *Marine Geology* 190:445–463, http://dx.doi.org/10.1016/S0025-3227(02)00358-4.

Yalciner, A.C., P. Gülkan, D.I. Dilmen, B. Aytore, A. Ayca, I. Insel, and A. Zaytsev. In press. Evaluation of tsunami scenarios for western Peloponnese, Greece. *Bollettino di Geofisica Teorica ed Applicata*, http://dx.doi.org/10.4430/bgta0126.

Yalciner, A.C., C. Ozer, H. Karakus, A. Zaytsev, and I. Guler. 2010. Evaluation of coastal risk at selected sites against Eastern Mediterranean tsunamis. *Coastal Engineering Proceedings* 1(32), management.10, http://dx.doi.org/10.9753/icce.v32.management.10.

Yalciner, A.C., E.N. Pelinovsky, E. Okal, and C.E. Synolakis, eds. 2003. *Submarine Landslides and Tsunamis*. NATO Science Series, vol. 21, Springer, 328 pp., http://dx.doi.org/10.1007/978-94-010-0205-9.

Yalciner, A.C., E. Pelinovsky, A. Zaytsev, A. Kurkin, C. Ozer, and H. Karakus. 2006. NAMI DANCE Manual. Middle East Technical University, Civil Engineering Department, Ocean Engineering Research Center, Ankara, Turkey, http://namidance.ce.metu.edu.tr/pdf/NAMIDANCE-version-5-9-manual.pdf.

Yalciner, A., E. Pelinovsky, A. Zaytsev, C. Ozer, A. Kurkin, H. Karakus, and G. Ozyurt. 2007. Modeling and visualization of tsunamis: Mediterranean examples. Pp. 273–283 in *Tsunami and Nonlinear Waves*. Springer, http://dx.doi.org/10.1007/978-3-540-71256-5_13.

Zahibo, N., E. Pelinovsky, A. Yalciner, A. Kurkin, A. Koselkov, and A. Zaitsev. 2003. The 1867 Virgin Island tsunami: Observations and modelling. *Oceanologica Acta* 26:609–621, http://dx.doi.org/10.1016/S0399-1784(03)00059-8.